HHS Public Access

Author manuscript

Nat Cell Biol. Author manuscript; available in PMC 2015 October 20.

Published in final edited form as:

Nat Cell Biol. 2015 July ; 17(7): 893–906. doi:10.1038/ncb3192.

Molecular characterization of LC3-associated phagocytosis (LAP) reveals distinct roles for Rubicon, NOX2, and autophagy proteins

Jennifer Martinez[1,7], **RK Subbarao Malireddi**[1], **Qun Lu**[2], **Larissa Dias Cunha**[1], **Stephane Pelletier**[1,3], **Sebastien Gingras**[1,3], **Robert Orchard**[2], **Jun-Lin Guan**[4], **Haiyan Tan**[5], **Junmin Peng**[5,6], **Thirumala-Devi Kanneganti**[1], **Herbert W. Virgin**[2], and **Douglas R. Green**[1]

[1]Department of Immunology, St. Jude Children's Research Hospital, Memphis, Tennessee 38105, USA

[2]Department of Pathology and Immunology, Washington University School of Medicine, St. Louis, MO 63110, USA

[3]Embryonic Stem Cell Laboratory, St. Jude Children's Research Hospital, Memphis, Tennessee 38105, USA

[4]Department of Cancer Biology, University of Cincinnati College of Medicine, Cincinnati, Ohio 45267

[5]St. Jude Proteomics Facility, St. Jude Children's Research Hospital, Memphis, Tennessee 38105, USA

[6]Departments of Structural Biology and Developmental Neurobiology, St. Jude Children's Research Hospital, Memphis, Tennessee 38105, USA

Abstract

LC3-associated phagocytosis (LAP) is a process wherein elements of canonical autophagy conjugate LC3 to the membranes of phagosomes, facilitating maturation upon fusion to lysosomes. Here, we characterize the molecular requirements for LAP, and identify a protein, Rubicon, required for LAP but not canonical autophagy. During LAP, Rubicon is recruited to the LAP-engaged phagosome ("LAPosome") and is required for the activity of a Class III PI3K complex containing Beclin-1, UVRAG, and VPS34, but lacking the canonical autophagy components ATG14 and Ambra1. This allows for the sustained localization of PI(3)P, which is critical for the recruitment of downstream autophagic proteins and the stabilization of the NOX2 complex to produce ROS. Both PI(3)P and ROS, as well as ATG7, ATG3, ATG5, ATG12, and ATG16L, are required for the conjugation of LC3 to the LAPosome and subsequent association

Correspondence should be addressed to: Douglas R. Green, Department of Immunology, MS #351, St Jude Children's Research Hospital, 262 Danny Thomas Place, Memphis TN 38105-2794, USA, Tel: (901) 595-3488; FAX: (901) 595-5766, douglas.green@stjude.org.

[7]Current address: Immunity, Inflammation, and Disease Laboratory, NIEHS, National Institutes of Health, Research Triangle Park, North Carolina, United States of America.

Contributions

J.M., T.D.K., H.W.V., and D.R.G. designed the experiments; J.M. performed and analyzed the experiments; S.M., Q. L., L.D.C., R.O., H.T., and J.P. performed and analyzed specific experiments; S.P. and S.G. performed CRISPR/Cas9 technology; J.L.G. contributed materials; and J.M., H.W.V., and D.R.G wrote the manuscript.

with LAMP1$^+$ lysosomes. LAP is also induced by engulfment of *Aspergillus fumigatus*, a fungal pathogen that commonly afflicts immunocompromised hosts, and is required for its optimal clearance *in vivo*. Therefore, we have identified molecules that distinguish LAP from canonical autophagy, thereby elucidating the importance of LAP in the response to *Aspergillus fumigatus* infection.

Introduction

Macroautophagy (herein, autophagy) is a catabolic, cell survival mechanism activated during nutrient scarcity involving the degradation and recycling of unnecessary or dysfunctional cellular components[1]. The proteins of the autophagy machinery often interact with pathogens, such as *Salmonella enterica, Listeria monocytogenes, Mycobacterium tuberculosis, Aspergillus fumigatus*[2], and *Shigella flexneri*[3], and function to quarantine and degrade the invading organism (xenophagy)[3]. LC3, the mammalian homologue of Atg8, is the most commonly monitored autophagy-related protein, and its lipidated form, LC3-II, is present on autophagosomes during canonical autophagy[4].

LC3-associated phagocytosis (LAP) is a process triggered upon phagocytosis of particles that engage cell surface receptors such as TLR1/2, TLR2/6, TLR4, TIM4, and FcR[5–7], resulting in the recruitment of some, but not all, members of the autophagic machinery to the stimulus-containing phagosome[6,8,9], facilitating rapid phagosome maturation, degradation of engulfed pathogens, and modulation of the immune response[5–10]. We[6–8] and others[9] have demonstrated that LAP and autophagy are functionally and mechanistically distinct processes. While the autophagosome is a double membrane structure, the LAP-engaged phagosome (LAPosome) is composed of a single membrane[5,8,11]. Autophagy requires the activity of the pre-initiation complex[12], while LAP proceeds independently of the pre-initiation complex[7,8]. However, LAP requires some autophagic components, such as the Class III PI3K complex[7,11], and elements of the ubiquitinylation-like, protein conjugation system (ATG5, ATG7[5–7,9,13]).

There remains a significant gap in our ability to differentiate the LAP pathway from canonical autophagy, in terms of molecular mechanisms and specificity. Here we identify the Class III PI3K-associated protein, Rubicon, as a molecule required for LAP, yet non-essential (indeed, inhibitory) for autophagy. Rubicon facilitates VPS34 activity and sustained PI(3)P presence on the LAPosome and stabilizes the NOX2 complex for ROS production, both of which are critical for the progression of LAP. Furthermore, Rubicon and the LAP pathway function in the clearance of *Aspergillus fumigatus*, a fungal pathogen that commonly infects immunocompromised hosts.

Results

Rubicon is required for LAP

We used a Stable Isotopy Labeling of Amino acids in Cell culture (SILAC)-based approach to profile the proteome of LAPosomes upon engulfment of inert beads versus beads conjugated to Pam3csk4 or IgG[6,8]. From this study, we identified Rubicon (RUN domain

protein as Beclin-1 interacting and cysteine-rich containing) as a protein associated with LAPosomes but not conventional phagosomes (Supplementary Table 1). Rubicon associates constitutively with the UVRAG-containing Class III PI3K complex[14]. Silencing of Rubicon results in an increase in the number of autophagosomes, indicating that Rubicon negatively regulates autophagy, via its inhibition of VPS34[14,15] or by blocking GTPase Rab7 activation[16] in autophagosome maturation.

We silenced Rubicon using shRNA in RAW-GFP-LC3[5] cells and observed that Rubicon-shRNA treatment abrogated the recruitment of GFP-LC3 to the phagosome, yet enhanced the formation of GFP-LC3^{+} puncta upon autophagy induction with rapamycin, as previously reported[14] (Figure 1a). Immunofluorescent staining revealed that endogenous LC3 was recruited to LAPosomes, in a manner similar to GFP-LC3 (Supplementary Figure 1a).

The recruitment of the LAP proteins to LAPosomes is a process distinct from conventional phagocytosis, as phagosomes containing inert beads fail to contain LAP-associated proteins (Supplementary Figure 1b). Time-lapse imaging of GFP-LC3 recruitment to the LAPosome showed that approximately 73% of zymosan-containing LAPosomes were GFP-LC3^{+}, compared to 3% of inert bead-containing phagosomes (Supplementary Figure 1c). We also used flow cytometry to quantify the amount of lipidated GFP-LC3 (LC3-II) associated with LAPosomes. Brief digitonin treatment resulted in the release of non-lipidated GFP-LC3 (LC3-I) from the cell, and thus the only GFP-LC3 detected after digitonin treatment was LC3-II, as confirmed by western blot analysis (Supplementary Figure 1d).

To characterize the role of Rubicon in LAP, we used CRISPR/Cas9-mediated gene targeting[17–19] to generate a Rubicon-deficient (Rubicon$^{-/-}$) mouse. This targeting successfully deleted Rubicon expression from all tissues examined (Supplementary Figure 2a–b). We obtained viable, fertile Rubicon$^{-/-}$ animals at Mendelian ratios (Supplementary Figure 2c). Rubicon$^{-/-}$ mice exhibited normal numbers of B cells, T cells, and NK cells in their spleens and lymph nodes and normal T cell subsets in their thymuses (Supplementary Figure 2d–f).

Bone marrow-derived macrophages from GFP-LC3-transgenic[20] Rubicon$^{+/+}$ and Rubicon$^{-/-}$ littermates were examined for their capacity to undergo canonical autophagy and LAP. In agreement with previous studies[14,15], rapamycin-treated or nutrient-deprived Rubicon$^{-/-}$ macrophages exhibited increased numbers of LC3 puncta, compared to wild-type macrophages (Figure 1b–d). However, Rubicon$^{-/-}$ macrophages were unable to translocate LC3 to the LAPosome, despite equivalent phagocytosis (Figure 1b–d, Supplementary Figure 2g). Previous work indicates that during autophagy, Rubicon prevents endosome maturation via binding to GTP-bound RAB7[16]. However, LAPosomes from both scrambled and RAB7 siRNA-treated RAW cells contained Rubicon upon LAP stimulation (Supplementary Figure 2h). Therefore, the recruitment of Rubicon to the LAPosome is independent of RAB7.

Purified LAPosomes from Rubicon$^{+/+}$ macrophages contained Beclin-1, UVRAG, VPS34, and Rubicon to the LAPosome as detected by immunoblot (Figure 1e). However, in the absence of Rubicon, Beclin1, UVRAG, and VPS34 recruitment was reduced, suggesting that

Rubicon plays a role in the retention of the complex at the LAPosome. Recruitment of ATG7 and LC3-II were also compromised in Rubicon$^{-/-}$ macrophages (Figure 1e).

We next examined the recruitment of Rubicon to the LAPosome in the absence of components of the pre-initiation complex (ULK1 and FIP200) or the Class III PI3K complex (Beclin1, VPS34). Beclin1, VPS34, UVRAG, Rubicon, and LC3-II were associated with LAPosomes from wild-type, ULK1$^{-/-}$, and LysM-Cre^{+} FIP200$^{flox/flox}$ macrophages (Supplementary Figure 3a–d). In the absence of VPS34, no recruitment to the LAPosome was observed for Beclin1, UVRAG, or Rubicon (Figure 1f). These data indicate that the stability of the Class III PI3K complex relies on VPS34, consistent with data demonstrating that loss of VPS34 results in the loss of the Class III PI3K complex as a whole in autophagy[21]. VPS34 and Rubicon, but not UVRAG, were present on the LAPosome in the absence of Beclin1 (Figure 1f). Therefore, while the formation and stability of the Class III PI3K complex is dependent on VPS34 and Beclin1, VPS34 appears to play a role in targeting the complex to the LAPosome.

We examined the ability of macrophages from genetically-deficient animals to generate PI(3)P, which is crucial for the recruitment of the downstream autophagic machinery[22]. Both wild-type and LysM-Cre+ FIP200$^{flox/flox}$ macrophages displayed increased VPS34 activity associated with the LAPosome (Figure 1g). LysM-Cre+ Beclin1$^{flox/flox}$, LysM-Cre+ VPS34$^{flox/flox}$, and Rubicon$^{-/-}$ macrophages did not demonstrate any VPS34 activity associated with the LAPosome (Figure 1g). As expected, LysM-Cre+ ATG5$^{flox/flox}$ macrophages displayed wild-type levels of VPS34 activity on the LAPosome (Figure 1g). These data indicate that while Rubicon inhibits VPS34 activity during canonical autophagy[14,15], VPS34 activity on the LAPosome requires Rubicon.

LAP utilizes a UVRAG-containing Class III PI3K complex

Canonical autophagy requires the activation of the pre-initiation complex, comprised of ULK1/2, FIP200, and ATG13[12], while LAP does not[8,9]. LysM-Cre^{+} FIP200$^{flox/flox}$ macrophages translocate LC3 to the LAPosome but are unable to form LC3 puncta in response to rapamycin or starvation (Supplementary Figure 3a–c). This result is consistent with the observation that FIP200 is not required for PI3K complex activity on the LAPosome (Figure 1g). Canonical autophagy requires the ULK1-dependent release of a Beclin1-activating cofactor, Ambra1, from the dynein motor complex[23], and the function of WIPI2[24]. Scrambled control, Ambra1 siRNA-treated, and WIPI2 siRNA-treated RAW-GFP-LC3 cells[5] were competent for LAP but Ambra1-silenced cells were unable to undergo autophagy in response to rapamycin or starvation (Supplementary Figure 3e–h). These data support the idea that LAP does not require the activity of the pre-initiation complex[6–9], Ambra1, or WIPI2.

While all Class III PI3K complexes contain Beclin1, VPS34, and VPS15, it can differ in additional components[25]. We confirmed the requirement for Beclin1 in LAP using LysM-Cre^{+} Beclin1$^{flox/flox}$ macrophages, which failed to translocate LC3 to LAPosomes or form GFP-LC3 puncta in response to autophagic stimuli (Figure 2a–b, Supplementary Figure 4a–b). The presence of PI(3)P on LAPosomes has been described[5], and using LysM-Cre^{+}

VPS34$^{flox/flox}$ macrophages, we found that VPS34 is required for LAP, as well as autophagy (Figure 2c–d, Supplementary Figure 4c–d).

ATG14 and UVRAG are mutually exclusive in their association with the Class III PI3K complex during autophagy[26], and silencing of either ATG14[15,26] or UVRAG[27] inhibits canonical autophagy. We examined the effect of silencing ATG14 or UVRAG on the translocation of LC3 to LAPosomes. Both LysM-Cre^{+} ATG14$^{flox/flox}$ macrophages and UVRAG siRNA-treated RAW-GFP-LC3 cells demonstrated defective autophagy in response to rapamycin or starvation. LysM-Cre^{+} ATG14$^{flox/flox}$ macrophages were able to translocate LC3 to the LAPosome, indicating that LAP does not require ATG14 (Figure 2e–f, Supplementary Figure 4e–f). Conversely, UVRAG siRNA-treated RAW-GFP-LC3 cells were compromised in their ability to undergo LAP, as well as canonical autophagy (Figure 2g–j, Supplementary Figure 4g–h).

While wild-type macrophages translocated Beclin1, UVRAG, Rab5, ATG7, and LC3-II to the LAPosome, ATG14 was not present on the LAPosome, despite high expression in cell lysates (Figure 2i). Beclin1-deficient macrophages failed to recruit UVRAG or any other downstream components of the LAP pathway to the LAPosome (Figure 2i). Likewise, WT macrophages robustly recruited Beclin-1, UVRAG, and VPS34, but not ATG14, to the LAPosome as detected by immunofluorescence (Supplementary Figure 4i–j). These data clearly demonstrate that while multiple Class III PI3K complexes are utilized by canonical autophagy[26], the LAP pathway only requires the activity of the UVRAG-containing Class III PI3K complex, with which Rubicon associates. We conclude that the activity of the UVRAG-containing, ATG14-deficient Class III PI3K complex involved in LAP depends on the presence of Rubicon.

NOX2 is downstream of the Class III PI3K complex and is required for LAP

NADPH oxidase-2 (NOX2, or gp91PHOX) is the only NADPH oxidase expressed in phagocytes[28]. NOX2 and p22PHOX are constitutively associated and located primarily in the membranes of intracellular vesicles. Generation of reactive oxygen species (ROS) requires translocation of cytosolic factors, p47PHOX, p40PHOX, p67PHOX, and Rac to the NOX2/p22PHOX complex[28]. Signaling via TLR or FcγR during phagocytosis can activate the assembly of the NOX2 complex and produce superoxide in the phagosomal lumen[29]. NOX2 has been linked to translocation of LC3 to TLR- or FcγR-engaged phagosomes and appears to play a signaling role in the recruitment of autophagy machinery to a localized target[10]. We similarly observed that NOX2$^{-/-}$ macrophages were unable to undergo LAP, yet were able to engage canonical autophagy in response to rapamycin or starvation (Figure 3a–b, Supplementary Figure 5a).

Previous reports suggested that NOX2-mediated ROS production is upstream of the function of Beclin1[10]. However, NOX2$^{-/-}$, LysM-Cre^{+} VPS34$^{flox/flox}$, and LysM-Cre^{+} Beclin1$^{flox/flox}$ macrophages all failed to produce ROS in response to zymosan stimulation (Figure 3c–d, Supplementary Figure 5b). Macrophages deficient for FIP200 or ATG7 were capable of producing ROS in response to zymosan (Figure 3d, Supplementary Figure 5b). Further, Rubicon$^{-/-}$ macrophages also failed to produce ROS in response to zymosan (Figure 3e, Supplementary Figure 5b), and Rubicon was effectively recruited to the

LAPosome in wild-type and NOX2$^{-/-}$ macrophages, but reduced in phagosomes from LysM-Cre^{+} Beclin1$^{flox/flox}$ macrophages (Figure 3f). Immunofluorescent staining revealed that LAPosomes from NOX2$^{-/-}$ macrophages contain wild-type levels of Beclin1, UVRAG, and VPS34 (Supplementary Figure 4i–j). NOX2$^{-/-}$ macrophages also displayed wild-type levels of VPS34 activity (Supplementary Figure 5c). Finally, ATG5-ATG12 and ATG16L, members of the downstream conjugation systems in autophagy[22], were recruited to LAPosomes in wild-type macrophages, but absent from those from Rubicon−/− and NOX2−/− macrophages (Figure 3g). These data place NOX2 and its activity downstream of the Class III PI3K complex and upstream of ATG7 in the process of LAP.

In addition to its interaction with the Class III PI3K complex, Rubicon can also translocate to the NOX2 complex upon zymosan stimulation[13]. Rubicon directly interacts with the p22PHOX subunit of NOX2 via its serine-rich domain (aa 567–625), a domain separate from the CCD domain (aa 515–550) responsible for its interaction with Beclin1[13] and the RUN domain (aa 49–180) responsible for its interaction with VPS34[30]. Rubicon stabilizes NOX2, resulting in maximal ROS production[13]. Of note, the p40PHOX subunit of NOX2 is a PI(3)P binding protein, and its ability to translocate to the NOX2 complex on the phagosome is impaired in the presence of wortmannin, an inhibitor of PI3K activity[31].

We therefore examined the assembly of the NOX2 complex in the absence of Class III PI3K complex components. Purified LAPosomes from wild-type and ULK1$^{-/-}$ macrophages contained the constitutively membrane associated subunit, p22PHOX, and the translocated, PI(3)P-binding subunit, phosphorylated p40PHOX (p-p40PHOX) (Figure 3f, Supplementary Figure 5d). LAPosomes from NOX2$^{-/-}$ macrophages contained dramatically reduced levels of both subunits, consistent with the role of NOX2 in the stability of its other components[28] (Figure 3f, Supplementary Figure 6a). While LAPosomes from LysM-Cre^{+} Beclin1$^{flox/flox}$ macrophages contained normal levels of p22PHOX, they lacked p-p40PHOX (Figure 3f). LAPosomes from Rubicon$^{-/-}$ macrophages also lacked p-p40PHOX, despite normal levels of p22PHOX (Figure 3h, Supplementary Figure 6a). Collectively, these data suggest that Rubicon promotes the association of the active Class III PI3K complex with the LAPosome, and stabilizes the NOX2 complex. VPS34 produces PI(3)P on the LAPosome, which further stabilizes the active NOX2 complex and promotes ROS production (Supplementary Figure 6b).

PI(3)P and ROS are both required for LAP

To examine the presence of PI(3)P on the LAPosome, bone marrow-derived macrophages were transiently transfected with a mCherry-fluorescent probe derived from the PX-domain of p40PHOX[32]. Whereas wild-type and NOX2$^{-/-}$ macrophages displayed equivalent levels of PI(3)P on the LAPosome, PI(3)P was not present on LAPosomes from LysM-Cre^{+} Beclin1$^{flox/flox}$, LysM-Cre^{+} VPS34$^{flox/flox}$, or Rubicon$^{-/-}$ macrophages (Figure 4a–b, Supplementary Figure 7a). Rubicon$^{-/-}$ macrophages displayed increased PX-mCherry^{+} puncta throughout the cell, indicative of increased VPS34 activity, compared to wild-type and other deficient macrophages (Figure 4b–c). These data suggest that in the absence of Rubicon, there exists an increased cellular level of VPS34 activity, as described[33], but Rubicon, is required to localize PI(3)P on the LAPosome.

One effect of ROS production is the oxidation of membrane lipids[34]. Immunofluorescent staining revealed that both wild-type and ULK1$^{-/-}$ macrophages displayed oxidized low-density lipoproteins (OxLDL) on the surface of LAPosomes, while LysM-Cre^{+} Beclin1$^{flox/flox}$ and NOX2$^{-/-}$ macrophages did not (Supplementary Figure 7a). PI(3)P decorated the LAPosome[5,6] of wild-type, ULK1−/−, and NOX2$^{-/-}$ macrophages, yet was absent from the LAPosomes of LysM-Cre^{+} Beclin1$^{flox/flox}$ macrophages (Supplementary Figure 7a). These data support the placement of NOX2 complex function downstream of the Class III PI3K complex in the LAP pathway.

We investigated the effect of pharmacologically-modulated ROS levels on the translocation of LC3 to the phagosome. RAW-GFP-LC3 cells were treated with the ROS inducer, *tert*-butyl hydroperoxide (TBHP), concurrently with inert beads. Co-treatment of inert beads with TBHP resulted in ROS production (Supplementary Figure 7b) and an increase in LC3-associated phagosomes (Figure 4d). Conversely, ROS production and LC3 translocation to zymosan- or Pam3csk4-bead-containing phagosomes was inhibited using Tiron, a ROS scavenger (Figure 4d, Supplementary Figure 7b–c). Similar effects were observed with 3-MA treatment, which inhibits VPS34 activity[5,8,35] (Figure 4d, Supplementary Figure 7b–c).

We next fed horseradish peroxidase (HRP)-coated latex beads to RAW-GFP-LC3 cells to induce intraphagosomal ROS production in the absence of a LAP engagement signal. This resulted in both ROS production (Supplementary Figure 7d) and LC3 translocation to the bead-containing phagosome (Figure 4e). Both wild-type and NOX2$^{-/-}$ macrophages were able to translocate GFP-LC3 to the HRP-bead-containing phagosome, whereas LysM-Cre^{+} Beclin1$^{flox/flox}$, LysM-Cre^{+} VPS34$^{flox/flox}$, and Rubicon$^{-/-}$ macrophages were not (Figure 4e). These data suggest that while Rubicon is needed for ROS production, exogenous ROS does not bypass the need for Rubicon, consistent with its requirement for PI(3)P generation.

LAP was analyzed in response to beads coupled to Pam3csk4 or to Pam3csk4 and catalase (which reduces H_2O_2 to H_2O_{36}), which successfully reduced ROS levels during LAP (Supplementary Figure 7e). Beads coated with both Pam3csk4 and catalase failed to recruit LC3 to the phagosome (Figure 4f–g). Therefore, both PI(3)P and ROS are required for successful LAP, and modulation of these signaling molecules can affect the outcome during phagocytosis.

LAP-induced phagosome maturation requires LC3-II

The translocation of LC3-II to the LAPosome is also a defining characteristic of LAP[4]. There exist at least three families of LC3-related proteins: microtubule-associated protein 1 light chain 3 (LC3, including LC3A, LC3B and LC3C); Golgi-associated ATPase enhancer of 16 kDa (GATE16); and γ-aminobutyric-acid-type-A ($GABA_A$)-receptor-associated protein (GABARAP). Members of all three families have been identified on autophagosomes[37]. SILAC analysis revealed that LC3B, GABARAP, and GATE16 associated with LAPosomes (Supplementary Table 1). Immunoblot analysis (Figure 5a) confirmed that LC3A, LC3B, GABARAP, and GATE16 associated with LAPosomes containing Pam3csk4-conjugated beads.

The molecular mechanisms that mediate LC3 conjugation are well described for autophagy[22]. While both ATG7[5,8] and ATG5[7,8] are required for both autophagy and LAP, the roles of other the components of the conjugation systems in LAP are unknown. LysM-Cre^{+} ATG5$^{flox/flox}$, LysM-Cre^{+} ATG12$^{flox/flox}$, and LysM-Cre^{+} ATG16L$^{flox/flox}$ macrophages all failed to undergo both LAP, in response to zymosan, or autophagy, in response to rapamycin or starvation (Figure 5b–g). Macrophages expressing the murine ATG16L T316A mutation, homologous with the human polymorphism associated with Crohn's disease[38], however, displayed marginal defects in LAP and canonical autophagy, suggesting that this single-nucleotide polymorphism has little or no effect on the LAP pathway in murine bone marrow-derived macrophages (Figure 5h–i).

The conjugation of LC3 to lipid (LC3-II) requires processing of the LC3-precursor to LC3-I, a process mediated by ATG4[22]. ATG4B$^{+/+}$ macrophages displayed GFP-LC3 puncta formation in response to rapamycin or starvation conditions, as well as rapid translocation of GFP-LC3 to the LAPosome. ATG4B$^{-/-}$ macrophages, however, failed to undergo canonical autophagy or LAP (Figure 6a–b). Similarly, LysM-Cre^{+} ATG3$^{flox/flox}$ macrophages did not form GFP-LC3 puncta in response to autophagic stimuli, nor did they undergo LAP in response to zymosan stimulation (Figure 6c–d). However, ATG4B-or ATG3-deficient macrophages displayed equivalent levels of phagocytosis (Figure 6e–f).

The lipidated, membrane-associated LC3-II is associated with both the outer and inner autophagosomal membranes and remains on the autophagosome during its formation, its completion, and its fusion with the lysosome[39,40]. To determine the role of LC3 in the maturation of the LAPosome, we utilized the *Legionella pneumophila* effector protein, RavZ, which is a cysteine protease that specifically targets LC3-PE (LC3-II) and generates an unlipidated LC3 product that lacks the essential C-terminal glycine required for re-lipidation[41]. The presence of RavZ resulted in an absence of both LC3-II (Figure 6g) and LAMP1 (Figure 6h–i) on the LAPosome, while RavZ-GFP rapidly translocated to the LAPosome (Figure 6h–i). Cells expressing the nonfunctional mutant, RavZ^{C258A}-GFP, however, contained LC3-II^{+}, LAMP1^{+} LAPosomes (Figure 6g, j–k). Collectively, these data suggest that the ATG5-12 and LC3-PE conjugation systems function to target lipidated LC3-II to the phagosome during LAP and that LC3-II facilitates the fusion of LAPosomes to lysosomes.

Clearance of *Aspergillus fumigatus* requires LAP

Patients with X-linked chronic granulomatous disease (CGD) commonly have mutated or deleted gp91PHOX, p22PHOX, and p47PHOX NOX2 subunits[42]. These patients can develop colitis and are susceptible to invasive fungal infection, such as Aspergilliosis.[43]. Macrophages from p47PHOX$^{-/-}$ mice and blood monocytes from CGD patients display reduced translocation of LC3 to phagosomes containing *Aspergillus fumigatus* spores[2]. In order to examine the ability of *A. fumigatus* to induce LAP, macrophages from various genetically-modified animals were cultured with *A. fumigatus* spores *in vitro*. Both wild-type and LysM-Cre^{+} FIP200$^{flox/flox}$ macrophages recruited LC3 to the pathogen-containing phagosome. Macrophages deficient for Beclin1, Rubicon, NOX2, or ATG7 failed to translocate LC3 to the *A. fumigatus*-containing phagosome, suggesting that this pathogen

triggers the LAP pathway (Figure 7a, Supplementary Figure 8a). Notably, macrophages from all genotypes exhibited equivalent levels of phagocytosis (Supplementary Figure 8b). Wild-type and LysM-Cre^{+} FIP200$^{flox/flox}$ macrophages exhibited robust clearance (Figure 7b) and killing (Supplementary Figure 8c) of *A. fumigatus in vitro* after 2 and 8 hours. However, LysM-Cre^{+} Beclin1$^{flox/flox}$, NOX2$^{-/-}$, Rubicon$^{-/-}$, and LysM-Cre^{+} ATG7$^{flox/flox}$ macrophages, were less able to clear *A. fumigatus in vitro* (Figure 7b, Supplementary Figure 8c).

We then challenged mice intra-nasally with *A. fumigatus* and monitored for weight loss, local fungal growth, cytokine production, and lung histopathology. Wild-type, LysM-Cre^{+} FIP200$^{flox/flox}$, and ULK1$^{-/-}$ mice did not lose weight (Supplementary Figure 8d) and were able to control fungal growth at 3 and 7 days post-infection (Figure 7c). LysM-Cre^{+} Beclin1$^{flox/flox}$, Rubicon$^{-/-}$, and LysM-Cre^{+} ATG7$^{flox/flox}$ mice displayed mild weight loss (Supplementary Figure 8d) and were delayed in their ability to restrict fungal growth in the lung at 3 and 7 days post-infection (Figure 7c). Lung tissue was analyzed for up-regulation of inflammatory cytokine genes at day 3 post-infection by qPCR. Lungs from LysM-Cre^{+} Beclin1$^{flox/flox}$, Rubicon$^{-/-}$, and LysM-Cre^{+} ATG7$^{flox/flox}$ mice revealed increased levels of IL-1β, IL-6, IL-12(p40), and TNFα, compared to wild-type, LysM-Cre^{+} FIP200$^{flox/flox}$, and ULK1$^{-/-}$ mice (Figure 7d). This upregulation of pro-inflammatory cytokines was also evident in the serum at day 7, as LysM-Cre^{+} Beclin1$^{flox/flox}$, Rubicon$^{-/-}$, and LysM-Cre^{+} ATG7$^{flox/flox}$ mice all displayed increased serum levels of G-CSF, IL-1α, IL-1β, IL-6, and KC (Supplementary Figure 8e). Histological analysis of infected lungs revealed that LysM-Cre+ Beclin1$^{flox/flox}$, Rubicon$^{-/-}$, and LysM-Cre^{+} ATG7$^{flox/flox}$ exhibited increased presence of *Aspergillus fumigatus*, inflammation, and granulomas at days 3 and 7 post-infection, compared to wild-type, LysM-Cre+ FIP200$^{flox/flox}$, and ULK1$^{-/-}$ mice (Figure 7e–f). Collectively, these data demonstrate that LAP is critical for the efficient clearance of *Aspergillus fumigatus* and prevention of inflammation and granuloma formation.

Discussion

LAP is a unique pathway that links signaling during phagocytosis with recruitment of some members of the autophagy machinery. Here we found that LAP, like autophagy[11,22], requires the activity of the ATG5-12-16L and LC3-PE conjugation systems, and that the presence of LC3-II on the LAPosome is crucial for lysosomal fusion and maturation of the LAPosome[22,39]. These observations provide insight into the role of LC3-II on the LAPosome, demonstrating that LC3-II is an active partner in the maturation process (Figure 8).

We identified, in association with the Beclin1-VPS34-UVRAG-containing Class III PI3K complex[14], as a molecule required for LAP but not autophagy. While Class III PI3K complexes lacking Rubicon were present at the LAPosome at low levels, it appears that this association is not sufficient for PI(3)P generation or LAP to progress. The recruitment of the Beclin1-VPS34-UVRAG-Rubicon complex (active only in LAP) is required for activity of the downstream conjugation systems to proceed, and reduced levels of localized PI(3)P at the LAPosome were observed in Rubicon$^{-/-}$ macrophages. Our data suggest that a Class III

PI3K complex containing Rubicon and UVRAG is recruited to the LAPosome and promotes the generation of PI(3)P.

Rubicon is also an important partner in promoting the production of ROS via the NOX2 complex[13]. We and others[10] observed that NOX2 and ROS are required for LC3 translocation to the zymosan-containing phagosome. Further, ROS production in response to LAP stimuli requires Rubicon and the Class III PI3K complex. Consistent with previous reports[13,28,31,32], LAPosomes from Beclin1-, VPS34-, or Rubicon-deficient macrophages all displayed reduced levels of localized PI(3)P, and subsequently, the PI(3)P-binding subunit of the NOX2 complex, p-p40PHOX, failed to stably associate with these LAPosomes. Rubicon allows for sustained PI3K activity at the LAPosome, and stabilization of the NOX2 complex via its binding to p-p40PHOX. It is possible that Rubicon itself stabilizes the NOX2 complex, thus promoting ROS production[13], although our analysis cannot discriminate such an effect from its role in generating PI(3)P. Therefore, Rubicon mediates the crosstalk between the Class III PI3K and NOX2 complexes, resulting in lipid oxidation and PI(3)P generation, both required for conjugation of LC3 to the LAPosome.

There are multiple possible mechanisms by which ROS can promote LC3-II translocation. One study reports that ROS, in the form of H_2O_2, directly inhibits the deconjugating activity of the cysteine protease, ATG4, which can cleave LC3-II into LC3-I and release it from the membrane[33,44]. While this study reported ROS production under starvation conditions, we did not observe substantial ROS production with rapamycin or starvation. Further, inhibition of ROS resulted in a failure of ATG7 to translocate to the LAPosome, indicating that the role of ROS during LAP is likely to be independent of ATG4. Another effect of ROS production is the oxidation of membrane lipids[34], which can acquire uncharacteristic biological activities[45]. LAPosomes from WT and ULK1$^{-/-}$ macrophages contained robust levels of oxidized low-density lipoproteins (OxLDL), while LysM-Cre^{+} Beclin1$^{flox/flox}$ and NOX2$^{-/-}$ macrophages did not.

Previous work has demonstrated that LAP plays a critical role in the degradation of engulfed organisms, such as intraphagosomal yeast[5], and is also a key player in the processing of phagocytic cargo and shaping of the innate immune response[6,8,9]. We found that clearance of *Aspergillus fumigatus* requires LAP, but not canonical autophagy, and animals defective for LAP exhibit increased pathological inflammation, pro-inflammatory cytokines, and fungal burden *in vivo*. Significantly, CGD patients with defective components of the NOX2 complex (required for LAP) are often plagued by Aspergilliosis[43]. This suggests that the inflammation, granulomas, and infectious susceptibility associated with CGD may be partially attributable to a defect in LAP.

Defects in autophagic machinery have been linked with aberrant host defense, inflammatory disease, and age-related disorders[3,46–54]. While initial interpretation of the above studies implicates autophagy, it is possible that a defect in LAP, rather than autophagy, accounts for some of these pathological conditions. It appears that there are “cassettes” of autophagy proteins that function, or not, in the control of different infections[53,54], some of which may be attributable to LAP. Characterization of the molecular mechanisms of LAP, in terms of

its divergence from autophagy, will allow us examination of pathologies linked to the autophagic machinery in a new light.

Supplementary Material

Refer to Web version on PubMed Central for supplementary material.

Acknowledgements

We thank the veterinary pathology core lab (VPCL) at St. Jude for their work in processing of H&E and Gomorri slides. We also thank the Cliff Guy in the Department of Immunology for his help with confocal microscopy. We thank Mao Yang for assistance with maintenance of the mouse colony. This work was supported by research grants from the National Institutes of Health, the Lupus Research Institute, and ALSAC.

References

1. Levine B. Eating oneself and uninvited guests: autophagy-related pathways in cellular defense. Cell. 2005; 120:159–162. [PubMed: 15680321]
2. de Luca A, et al. IL-1 receptor blockade restores autophagy and reduces inflammation in chronic granulomatous disease in mice and in humans. Proc Natl Acad Sci U S A. 2014; 111:3526–3531. [PubMed: 24550444]
3. Levine B, Mizushima N, Virgin HW. Autophagy in immunity and inflammation. Nature. 2011; 469:323–335. [PubMed: 21248839]
4. Klionsky DJ, et al. Guidelines for the use and interpretation of assays for monitoring autophagy. Autophagy. 2012; 8:445–544. [PubMed: 22966490]
5. Sanjuan MA, et al. Toll-like receptor signalling in macrophages links the autophagy pathway to phagocytosis. Nature. 2007; 450:1253–1257. [PubMed: 18097414]
6. Henault J, et al. Noncanonical autophagy is required for type I interferon secretion in response to DNA-immune complexes. Immunity. 2012; 37:986–997. [PubMed: 23219390]
7. Kim JY, et al. Noncanonical autophagy promotes the visual cycle. Cell. 2013; 154:365–376. [PubMed: 23870125]
8. Martinez J, et al. Microtubule-associated protein 1 light chain 3 alpha (LC3)-associated phagocytosis is required for the efficient clearance of dead cells. Proceedings of the National Academy of Sciences of the United States of America. 2011; 108:17396–17401. [PubMed: 21969579]
9. Florey O, Kim SE, Sandoval CP, Haynes CM, Overholtzer M. Autophagy machinery mediates macroendocytic processing and entotic cell death by targeting single membranes. Nat Cell Biol. 2011; 13:1335–1343. [PubMed: 22002674]
10. Huang J, et al. Activation of antibacterial autophagy by NADPH oxidases. Proceedings of the National Academy of Sciences of the United States of America. 2009; 106:6226–6231. [PubMed: 19339495]
11. Mizushima N, Ohsumi Y, Yoshimori T. Autophagosome formation in mammalian cells. Cell structure and function. 2002; 27:421–429. [PubMed: 12576635]
12. Kim J, Kundu M, Viollet B, Guan KL. AMPK and mTOR regulate autophagy through direct phosphorylation of Ulk1. Nat Cell Biol. 2011; 13:132–141. [PubMed: 21258367]
13. Yang CS, et al. Autophagy protein Rubicon mediates phagocytic NADPH oxidase activation in response to microbial infection or TLR stimulation. Cell Host Microbe. 2012; 11:264–276. [PubMed: 22423966]
14. Matsunaga K, et al. Two Beclin 1-binding proteins, Atg14L and Rubicon, reciprocally regulate autophagy at different stages. Nat Cell Biol. 2009; 11:385–396. [PubMed: 19270696]
15. Zhong Y, et al. Distinct regulation of autophagic activity by Atg14L and Rubicon associated with Beclin 1-phosphatidylinositol-3-kinase complex. Nat Cell Biol. 2009; 11:468–476. [PubMed: 19270693]

16. Sun Q, Westphal W, Wong KN, Tan I, Zhong Q. Rubicon controls endosome maturation as a Rab7 effector. Proc Natl Acad Sci U S A. 2010; 107:19338–19343. [PubMed: 20974968]
17. Wang H, et al. One-step generation of mice carrying mutations in multiple genes by CRISPR/Cas-mediated genome engineering. Cell. 2013; 153:910–918. [PubMed: 23643243]
18. Ran FA, et al. Double Nicking by RNA-Guided CRISPR Cas9 for Enhanced Genome Editing Specificity. Cell. 2013; 154:1380–1389. [PubMed: 23992846]
19. Pelletier S, Gingras S, Green DR. Mouse Genome Engineering via CRISPR-Cas9 for Study of Immune Function. Immunity. 2015; 42:18–27. [PubMed: 25607456]
20. Mizushima N, Yamamoto A, Matsui M, Yoshimori T, Ohsumi Y. In vivo analysis of autophagy in response to nutrient starvation using transgenic mice expressing a fluorescent autophagosome marker. Molecular biology of the cell. 2004; 15:1101–1111. [PubMed: 14699058]
21. Willinger T, Flavell RA. Canonical autophagy dependent on the class III phosphoinositide-3 kinase Vps34 is required for naive T-cell homeostasis. Proceedings of the National Academy of Sciences of the United States of America. 2012; 109:8670–8675. [PubMed: 22592798]
22. Mizushima N. Autophagy: process and function. Genes & development. 2007; 21:2861–2873. [PubMed: 18006683]
23. Fimia GM, et al. Ambra1 regulates autophagy and development of the nervous system. Nature. 2007; 447:1121–1125. [PubMed: 17589504]
24. Polson HE, et al. Mammalian Atg18 (WIPI2) localizes to omegasome-anchored phagophores and positively regulates LC3 lipidation. Autophagy. 2010; 6:506–522. [PubMed: 20505359]
25. Levine B, Deretic V. Unveiling the roles of autophagy in innate and adaptive immunity. Nature reviews. 2007; 7:767–777.
26. Itakura E, Kishi C, Inoue K, Mizushima N. Beclin 1 forms two distinct phosphatidylinositol 3-kinase complexes with mammalian Atg14 and UVRAG. Molecular biology of the cell. 2008; 19:5360–5372. [PubMed: 18843052]
27. Song Z, et al. Essential role for UVRAG in autophagy and maintenance of cardiac function. Cardiovascular research. 2014; 101:48–56. [PubMed: 24081163]
28. Bedard K, Krause KH. The NOX family of ROS-generating NADPH oxidases: physiology and pathophysiology. Physiological reviews. 2007; 87:245–313. [PubMed: 17237347]
29. Suh CI, et al. The phosphoinositide-binding protein p40phox activates the NADPH oxidase during FcgammaIIA receptor-induced phagocytosis. J Exp Med. 2006; 203:1915–1925. [PubMed: 16880255]
30. Sun Q, et al. The RUN domain of rubicon is important for hVps34 binding, lipid kinase inhibition, and autophagy suppression. The Journal of biological chemistry. 2011; 286:185–191. [PubMed: 21062745]
31. Ueyama T, et al. Cooperation of p40(phox) with p47(phox) for Nox2-based NADPH oxidase activation during Fcgamma receptor (FcgammaR)-mediated phagocytosis: mechanism for acquisition of p40(phox) phosphatidylinositol 3-phosphate (PI(3)P) binding. The Journal of biological chemistry. 2011; 286:40693–40705. [PubMed: 21956105]
32. Kanai F, et al. The PX domains of p47phox and p40phox bind to lipid products of PI(3)K. Nat Cell Biol. 2001; 3:675–678. [PubMed: 11433300]
33. Yang Z, Klionsky DJ. An overview of the molecular mechanism of autophagy. Curr Top Microbiol Immunol. 2009; 335:1–32. [PubMed: 19802558]
34. Smith WL, Murphy RC. Oxidized lipids formed non-enzymatically by reactive oxygen species. The Journal of biological chemistry. 2008; 283:15513–15514. [PubMed: 18285325]
35. Wu YT, et al. Dual role of 3-methyladenine in modulation of autophagy via different temporal patterns of inhibition on class I and III phosphoinositide 3-kinase. The Journal of biological chemistry. 2010; 285:10850–10861. [PubMed: 20123989]
36. Thannickal VJ, Fanburg BL. Reactive oxygen species in cell signaling. Am J Physiol Lung Cell Mol Physiol. 2000; 279:L1005–L1028. [PubMed: 11076791]
37. Kabeya Y, et al. LC3, GABARAP and GATE16 localize to autophagosomal membrane depending on form-II formation. Journal of cell science. 2004; 117:2805–2812. [PubMed: 15169837]

38. Murthy A, et al. A Crohn's disease variant in Atg16l1 enhances its degradation by caspase 3. Nature. 2014; 506:456–462. [PubMed: 24553140]
39. Yorimitsu T, Klionsky DJ. Autophagy: molecular machinery for self-eating. Cell death and differentiation. 2005; 12(Suppl 2):1542–1552. [PubMed: 16247502]
40. Jager S, et al. Role for Rab7 in maturation of late autophagic vacuoles. Journal of cell science. 2004; 117:4837–4848. [PubMed: 15340014]
41. Choy A, et al. The Legionella effector RavZ inhibits host autophagy through irreversible Atg8 deconjugation. Science (New York, N.Y. 2012; 338:1072–1076.
42. Debeurme F, et al. Regulation of NADPH oxidase activity in phagocytes: relationship between FAD/NADPH binding and oxidase complex assembly. The Journal of biological chemistry. 2010; 285:33197–33208. [PubMed: 20724480]
43. Mamishi S, et al. A case of invasive aspergillosis in CGD patient successfully treated with Amphotericin B and INF-gamma. Annals of clinical microbiology and antimicrobials. 2005; 4:4. [PubMed: 15745454]
44. Scherz-Shouval R, et al. Reactive oxygen species are essential for autophagy and specifically regulate the activity of Atg4. The EMBO journal. 2007; 26:1749–1760. [PubMed: 17347651]
45. Bochkov VN, et al. Generation and biological activities of oxidized phospholipids. Antioxid Redox Signal. 2010; 12:1009–1059. [PubMed: 19686040]
46. Hampe J, et al. A genome-wide association scan of nonsynonymous SNPs identifies a susceptibility variant for Crohn disease in ATG16L1. Nat Genet. 2007; 39:207–211. [PubMed: 17200669]
47. Rioux JD, et al. Genome-wide association study identifies new susceptibility loci for Crohn disease and implicates autophagy in disease pathogenesis. Nat Genet. 2007; 39:596–604. [PubMed: 17435756]
48. Cadwell K, Stappenbeck TS, Virgin HW. Role of autophagy and autophagy genes in inflammatory bowel disease. Curr Top Microbiol Immunol. 2009; 335:141–167. [PubMed: 19802564]
49. Jo EK, Shin DM, Choi AM. Autophagy: cellular defense to excessive inflammation. Microbes Infect. 2012; 14:119–125. [PubMed: 21924374]
50. Harris J. Autophagy and cytokines. Cytokine. 2011; 56:140–144. [PubMed: 21889357]
51. Green DR, Galluzzi L, Kroemer G. Mitochondria and the autophagy-inflammation-cell death axis in organismal aging. Science (New York, N.Y. 2011; 333:1109–1112.
52. White E, Karp C, Strohecker AM, Guo Y, Mathew R. Role of autophagy in suppression of inflammation and cancer. Curr Opin Cell Biol. 2010; 22:212–217. [PubMed: 20056400]
53. Choi J, et al. The parasitophorous vacuole membrane of Toxoplasma gondii is targeted for disruption by ubiquitin-like conjugation systems of autophagy. Immunity. 2014; 40:924–935. [PubMed: 24931121]
54. Zhao Z, et al. Autophagosome-independent essential function for the autophagy protein Atg5 in cellular immunity to intracellular pathogens. Cell Host Microbe. 2008; 4:458–469. [PubMed: 18996346]

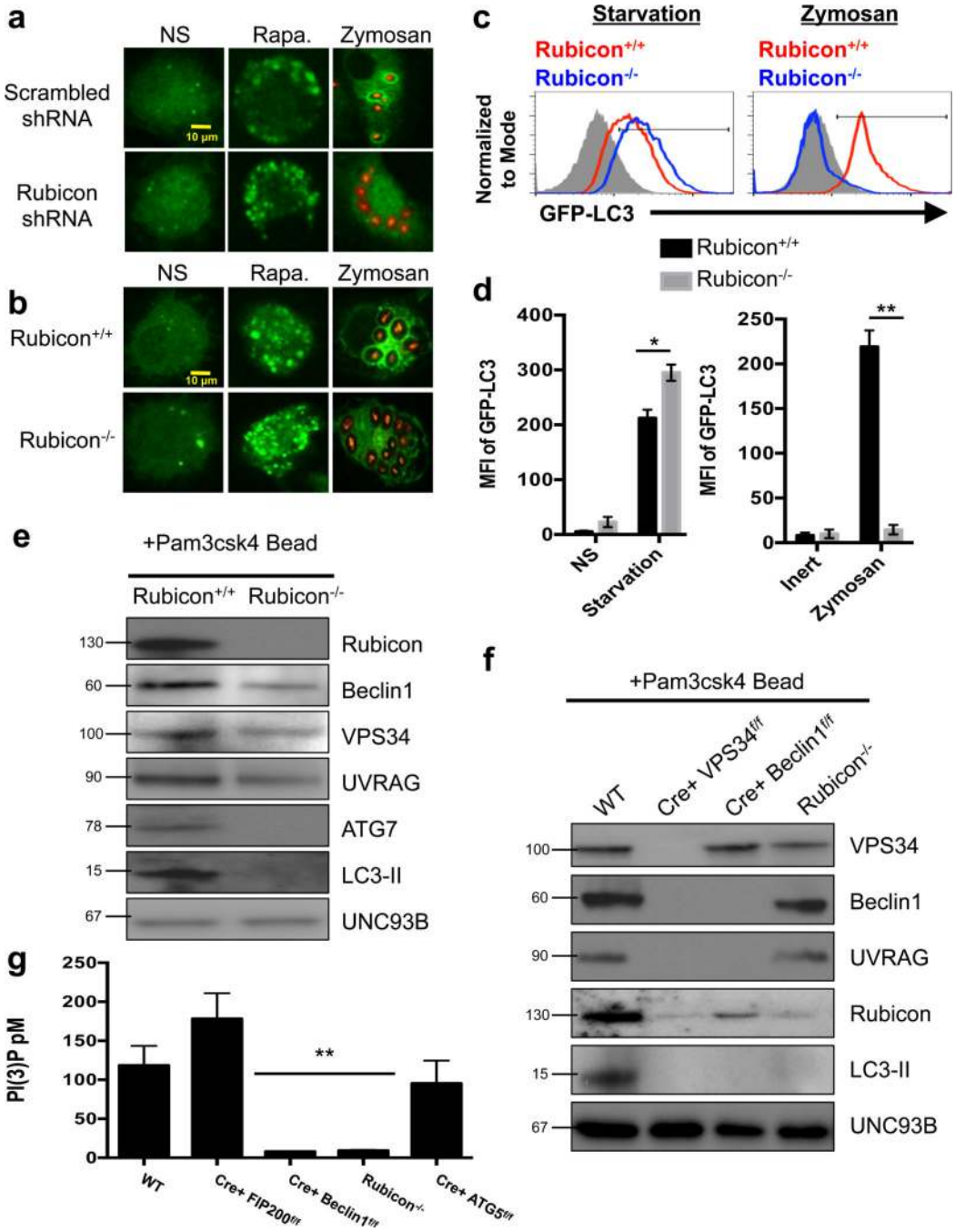

Figure 1. Rubicon is required for LAP

(**a**) RAW-GFP-LC3 cells were transduced with lentiviral constructs for Scrambled shRNA or Rubicon shRNA. At 72 hours after transfection, cells were left untreated (NS) or treated with 200 nM rapamycin (Rapa.) or fed Alexa Fluor 594-zymosan (Zymosan). GFP-LC3 puncta was assessed at 18 h, and translocation of GFP-LC3 to the LAPosome was assessed at 1 h. (**b–d**) Rubicon$^{+/+}$ GFP-LC3^{+} and Rubicon$^{-/-}$ GFP-LC3^{+} bone marrow-derived macrophages were left untreated (NS) or were cultured with 200 nM rapamycin (Rapa., **b**), starvation conditions (**c**), or Alexa Fluor 594-zymosan (Zymosan, **b–c**). GFP-LC3 puncta

was assessed at 18 h, and translocation of GFP-LC3 to the LAPosome was assessed at 1 h by confocal microscopy (**b**) and flow cytometry (**c**). Filled grey histogram represents inert bead. (**d**) The mean fluorescence intensity (MFI) of membrane bound GFP-LC3 was determined using flow cytometry under starvation conditions (left) and zymosan feeding (right). Data are presented as mean ± SD of three independent experiments (*$p < 0.05$, **$p < 0.001$). (**e–f**) Bone marrow-derived macrophages from Rubicon$^{+/+}$ and Rubicon$^{-/-}$ mice (**e**) or WT, LysM-Cre+ VPS34$^{flox/flox}$, LysM-Cre+ Beclin1$^{flox/flox}$, and Rubicon$^{-/-}$ mice (**f**) were allowed to phagocytose latex beads coated with Pam3csk4 for 1 hr. Phagosomes were purified using sucrose gradient as described in experimental procedures. Phagosome proteins were solubilized in SDS-PAGE and blotted with the indicated antibodies. The results presented are representative of three independent experiments. **(g)** Bone marrow-derived macrophages from genetic knockout strains were fed Pam3csk4-beads (30 minutes). mVPS34 was immunoprecipitated from the purified LAPosomes, and equivalent amounts were used in the Class III PI3K Activity assay. Data, as pM of PI(3)P, is presented as mean ± SD of three independent experiments (**$p < 0.001$).

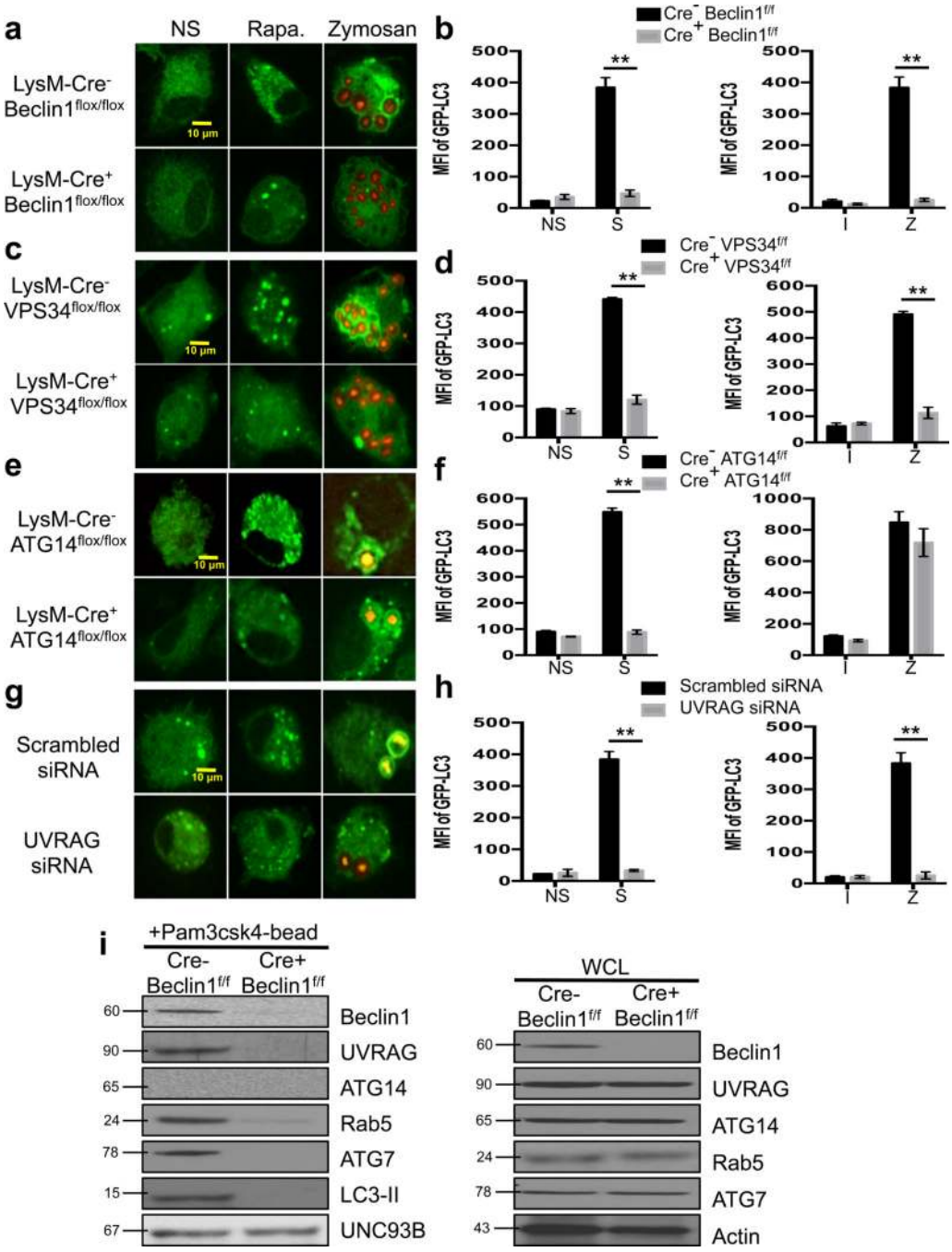

Figure 2. LAP utilizes a UVRAG-containing Class III PI3K Complex

(**a–b**) Bone marrow-derived macrophages from LysM-Cre– Beclin1$^{flox/flox}$ GFP-LC3^{+} and LysM-Cre+ Beclin1$^{flox/flox}$ GFP-LC3^{+} mice were left untreated (NS) or were cultured with 200 nM rapamycin (Rapa., **a**), starvation conditions (S, **b**), Inert beads (I, **b**), or Alexa Fluor 594-zymosan (Zymosan or Z, **a–b**). (**c–d**) Bone marrow-derived macrophages from LysM-Cre– VPS34$^{flox/flox}$ GFP-LC3^{+} and LysM-Cre+ VPS34$^{flox/flox}$ GFP-LC3^{+} mice were left untreated (NS) or were cultured with 200 nM rapamycin (Rapa., **c**), starvation conditions (S, **d**), Inert beads (I, **d**), or Alexa Fluor 594-zymosan (Zymosan or Z, **c–d**). (**e–f**) Bone

marrow-derived macrophages from LysM-Cre− ATG14$^{flox/flox}$ and LysM-Cre+ ATG14$^{flox/flox}$ mice were transfected with GFP-LC3. After 48 hours of transfection, cells were left untreated (NS) or were cultured with 200 nM rapamycin (Rapa., **e**), starvation conditions (S, **f**), Inert beads (I, **f**), or Alexa Fluor 594-zymosan (Zymosan or Z, **e–f**). (**g–h**) RAW-GFP-LC3 cells were transfected with Scrambled or UVRAG siRNA oligonucleotides. After 48 hours of transfection, cells were left untreated (NS) or were cultured with 200 nM rapamycin (Rapa., **g**), starvation conditions (S, **h**), Inert beads (I, **h**), or Alexa Fluor 594-zymosan (Zymosan or Z, **g–h**). GFP-LC3 puncta was assessed at 18 h, and translocation of GFP-LC3 to the LAPosome was assessed at 1 h by confocal microscopy (**a, c, e, g**) and flow cytometry (**b, d, f, h**). Data are presented as mean ± SD of three independent experiments (**p < 0.001). (**i**) Bone marrow-derived macrophages from LysM-Cre− Beclin1$^{flox/flox}$ and LysM-Cre+ Beclin1$^{flox/flox}$ mice were allowed to phagocytose latex beads coated with Pam3csk4 for 1 hr. Phagosomes were purified using sucrose gradient as described in experimental procedures. Phagosome proteins (left), as well as whole cell lysates from non-stimulated cells (right), were solubilized in SDS-PAGE and blotted with the indicated antibodies. The results presented are representative of three independent experiments.

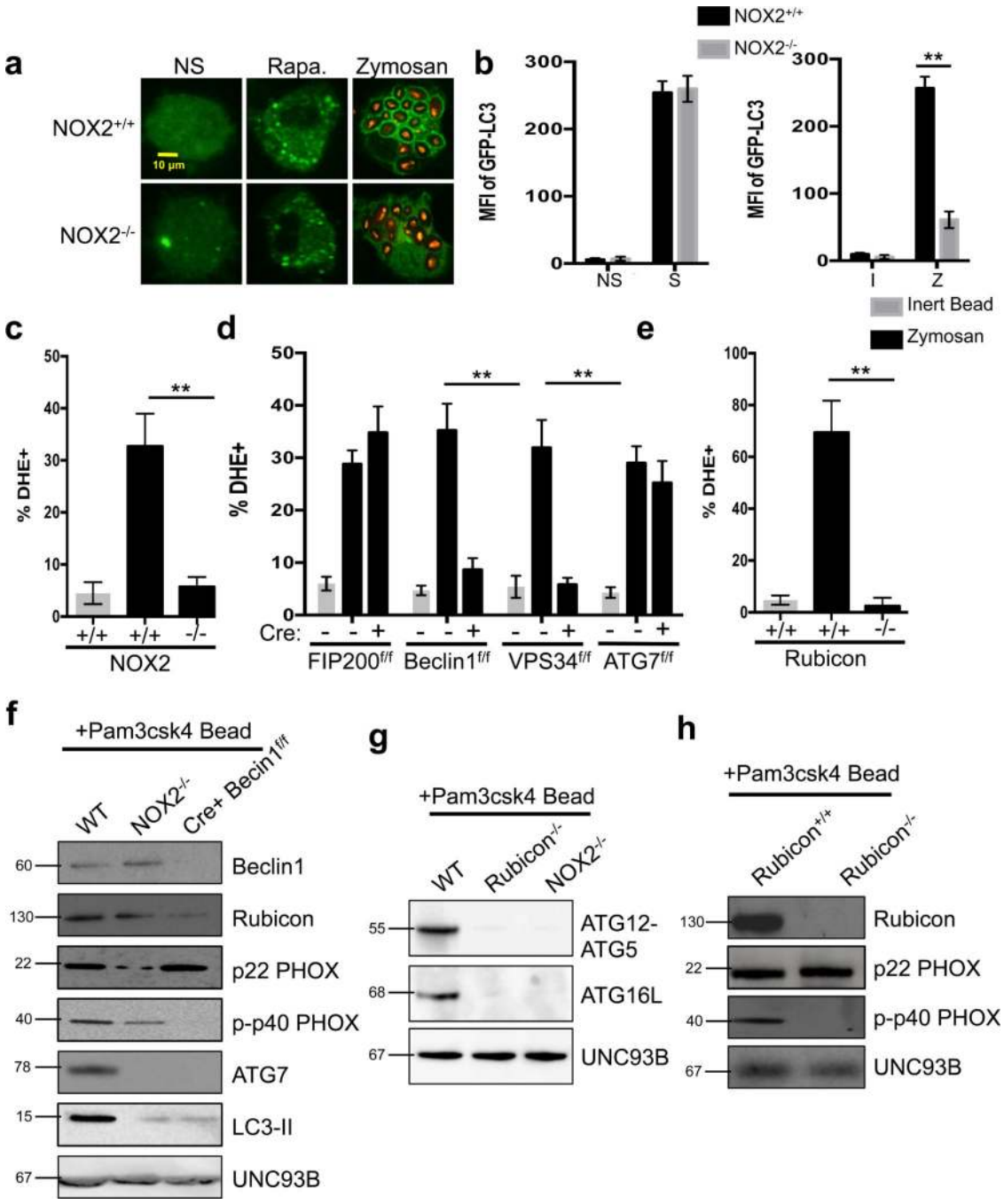

Figure 3. NOX2 is downstream of the Class III PI3K Complex and required for LAP

(**a–b**) Bone marrow-derived macrophages from NOX2$^{+/+}$ GFP-LC3^{+} and NOX2$^{-/-}$ GFP-LC3^{+} mice were left untreated (NS) or were cultured with 200 nM rapamycin (Rapa., **a**), starvation conditions (S, **b**), Inert beads (I, **b**), or Alexa Fluor 594-zymosan (Zymosan or Z, **a–b**). GFP-LC3 puncta was assessed at 18 h, and translocation of GFPLC3 to the LAPosome was assessed at 1 h by confocal microscopy (**a**) and flow cytometry (**b**). (**c–e**) Bone marrow-derived macrophages from genetic knockout strains were fed inert beads or Alexa Fluor 594-zymosan and analyzed for ROS production at 1 h by flow cytometry using

dihydroethidium (DHE). Data are presented as mean ± SD of three independent experiments (**p < 0.001). (**f–h**) Bone marrow-derived macrophages from WT, NOX2$^{-/-}$, and LysM-Cre+ Beclin1$^{flox/flox}$ mice (**f**), Rubicon$^{+/+}$ and Rubicon$^{-/-}$ mice (**g**), and WT, Rubicon$^{-/-}$, and NOX2$^{-/-}$ mice (**h**) were allowed to phagocytose latex beads coated with Pam3csk4 for 1 hr. Phagosomes were purified using sucrose gradient as described in experimental procedures. Phagosome proteins were solubilized in SDS-PAGE and blotted with the indicated antibodies. The results presented are representative of three independent experiments.

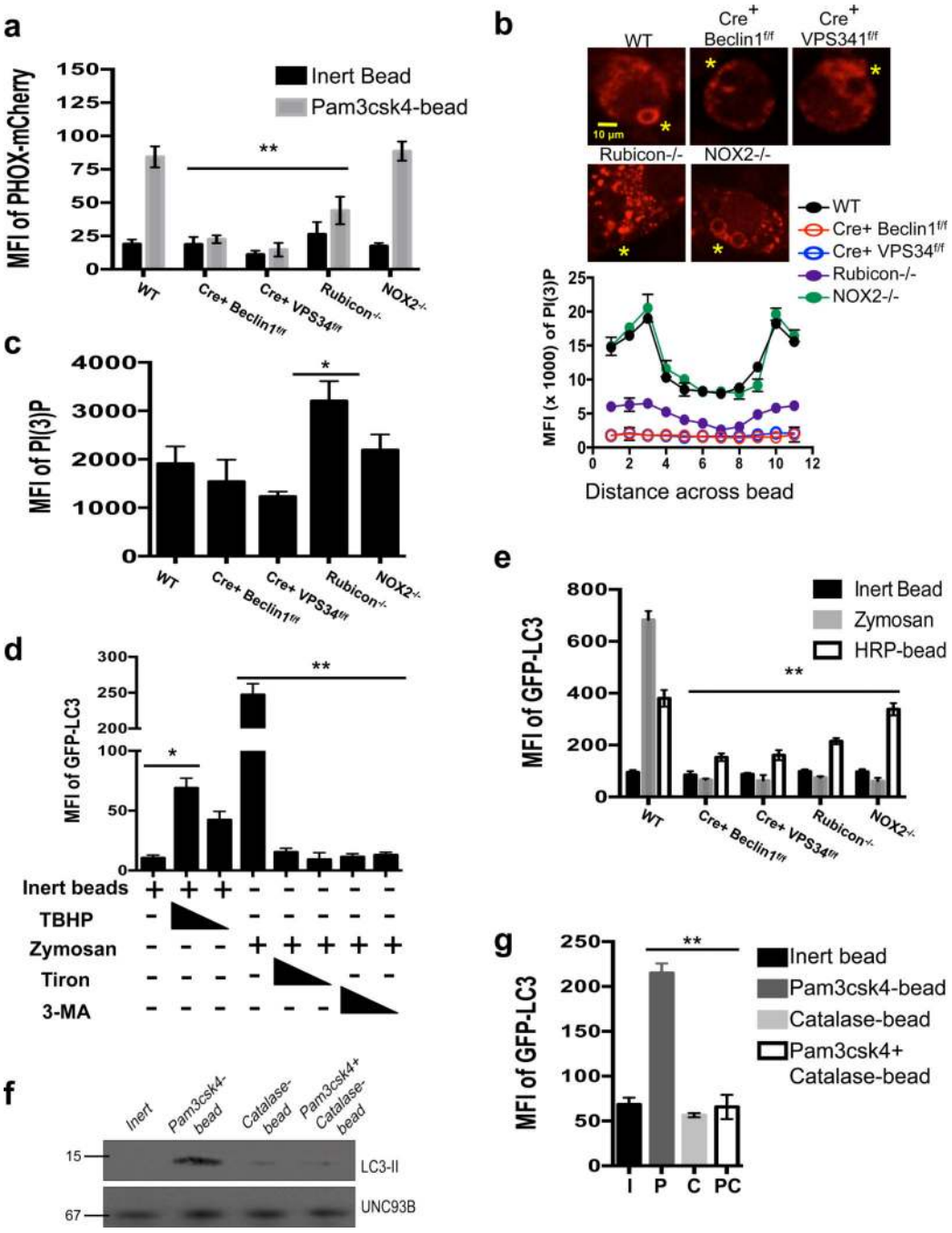

Figure 4. PI(3)P and ROS are both required for LAP

(**a–c**) Bone marrow-derived macrophages from genetic knockout strains were transiently transfected with PX-mCherry. After 48 hours of transfection, cells were fed inert beads or Pam3csk4-beads for 30 minutes. PI(3)P on LAPosomes was analyzed by flow cytometry (**a**) or confocal microscopy (**b–c**). Yellow asterisks indicate internalized beads. Representative images and signal intensity profiles for PX-mCherry across phagocytosed beads are quantified and shown graphically (n ≥25 / genotype) (**b**). Masks were generated around whole cells and the MFI of PI(3)P within the cell was quantified using Slidebook software.

Data are presented as mean ± SD of three independent experiments (**p < 0.001) (**c**). Data are presented as mean ± SD of two independent experiments (n ≥25 / genotype). (**d**) RAW-GFP-LC3 cells were fed inert beads or zymosan, in the presence or absence of *tert*-butyl hydroperoxide (TBHP, 100 μM, 50 μM), Tiron (1 mM, 0.5 mM), or 3-MA (25 mM, 5 mM). Translocation of GFP-LC3 to the LAPosome was assessed at 1 h by flow cytometry. (**e**) Bone marrow-derived macrophages from GFP-LC3^{+} genetic knockout strains were fed inert beads, Alexa Fluor 594-zymosan, or HRP-coupled beads. Translocation of GFP-LC3 to the LAPosome was assessed at 1 h by flow cytometry. Data are presented as mean ± SD of three independent experiments (**p < 0.001) (**f–g**) RAW-GFP-LC3 cells were fed inert beads (I), Pam3csk4-beads (P), Catalase-beads (C), or Pam3csk4+Catalase-beads (PC). Translocation of GFP-LC3 to the LAPosome was assessed at 1 h by immunoblot analysis of purified phagosomal proteins (**f**) and flow cytometry (**g**). Data are presented as mean ± SD of three independent experiments (**p < 0.001).

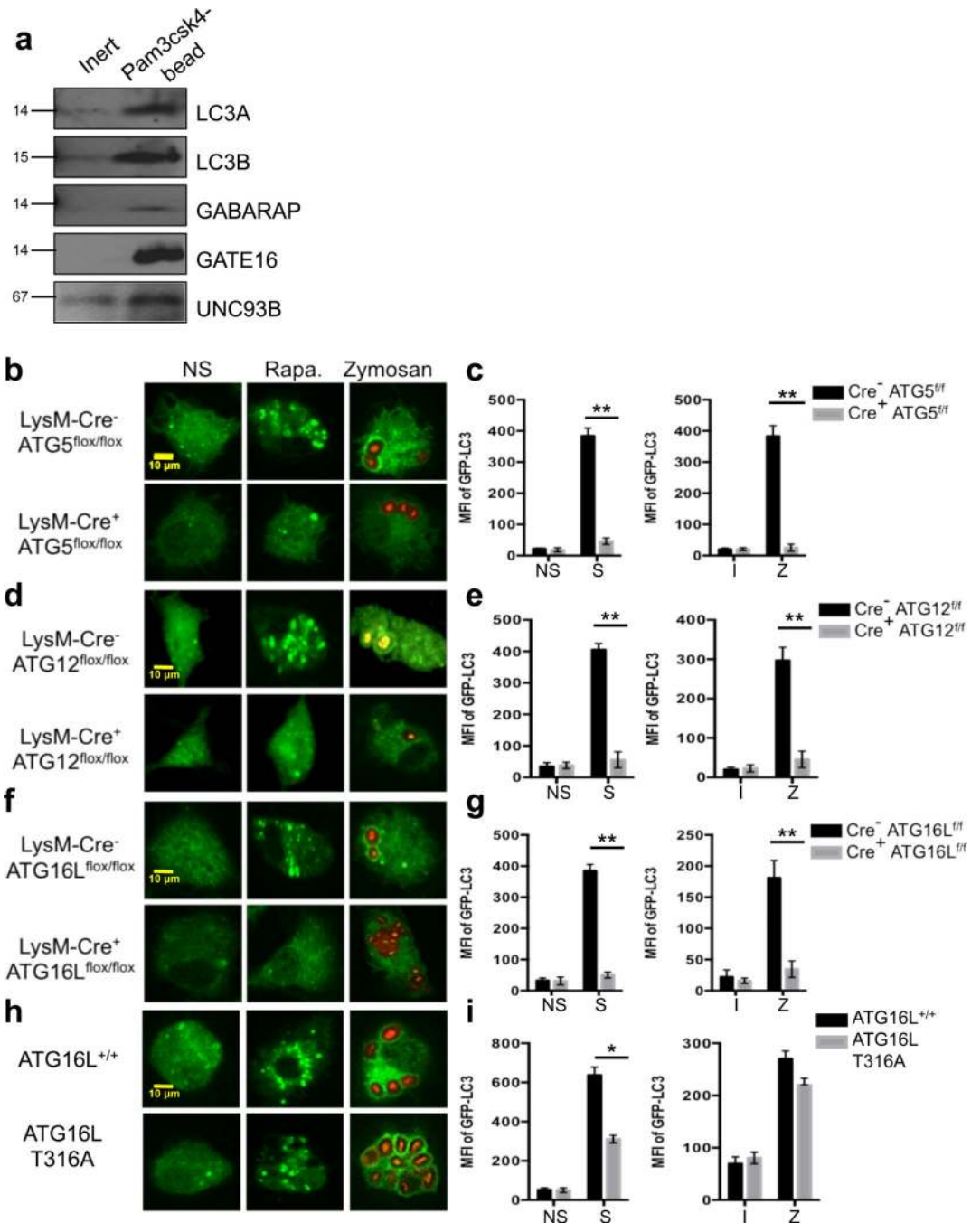

Figure 5. The ATG5-12-16L and LC3-PE conjugation systems are required for LAP

(**a**) RAW cells were allowed to phagocytose inert beads or Pam3csk4-beads for 1 hour. Phagosomes were purified using sucrose gradient as described in experimental procedures. Phagosome proteins (left), as well as whole cell lysates from non-stimulated cells (right), were solubilized in SDS-PAGE and blotted with the indicated antibodies. The results presented are representative of three independent experiments. (**b–c**) Bone marrow-derived macrophages from LysM-Cre– ATG5$^{flox/flox}$ GFP-LC3+ and LysM-Cre+ ATG5$^{flox/flox}$ GFP-LC3+ mice were left untreated (NS) or were cultured with 200 nM rapamycin (Rapa.,

b), starvation conditions (S, **c**), Inert beads (I, **c**), or Alexa Fluor 594-zymosan (Zymosan or Z, **b–c**). (**d–e**) Bone marrow-derived macrophages from LysM-Cre− ATG12$^{flox/flox}$ and LysM-Cre+ ATG12$^{flox/flox}$ mice were transfected with GFP-LC3. After 48 hours of transfection, cells were left untreated (NS) or were cultured with 200 nM rapamycin (Rapa., **d**), starvation conditions (S, **e**), Inert beads (I, **e**), or Alexa Fluor 594-zymosan (Zymosan or Z, **d–e**). (**f–g**) Bone marrow-derived macrophages from LysM-Cre− ATG16L$^{flox/flox}$ GFP-LC3^{+} and LysM-Cre+ ATG16L$^{flox/flox}$ GFP-LC3^{+} mice were left untreated (NS) or were cultured with 200 nM rapamycin (Rapa., **f**), starvation conditions (S, **g**), Inert beads (I, **g**), or Alexa Fluor 594-zymosan (Zymosan or Z, **f–g**). (**h–i**) Bone marrow-derived macrophages from ATG16L$^{+/+}$ and ATG16L T316A mice were transfected with GFP-LC3. After 48 hours of transfection, cells were left untreated (NS) or were cultured with 200 nM rapamycin (Rapa., **h**), starvation conditions (S, **i**), Inert beads (I, **i**), or Alexa Fluor 594-zymosan (Zymosan or Z, **h–i**). GFP-LC3 puncta was assessed at 18 h, and translocation of GFP-LC3 to the LAPosome was assessed at 1 h by confocal microscopy (**b, d, f, h**) and flow cytometry (**c, e, g, i**). (**j**) ATG4B$^{+/+}$ and ATG4B$^{-/-}$ macrophages were fed Alexa Fluor 594-zymosan, and the percent of phagocytosis (% Phagocytosis, left) and the extent of phagocytosis (MFI of Phagocytosed Zymosan, right) was quantified by flow cytometry. (**k**) LysM-Cre− ATG3$^{flox/flox}$ and LysM-Cre+ ATG3$^{flox/flox}$ macrophages were fed Alexa Fluor 594-zymosan, and the percent of phagocytosis (% Phagocytosis, left) and the extent of phagocytosis (MFI of Phagocytosed Zymosan, right) was quantified by flow cytometry. Data are presented as mean ± SD of three independent experiments (**$p < 0.001$).

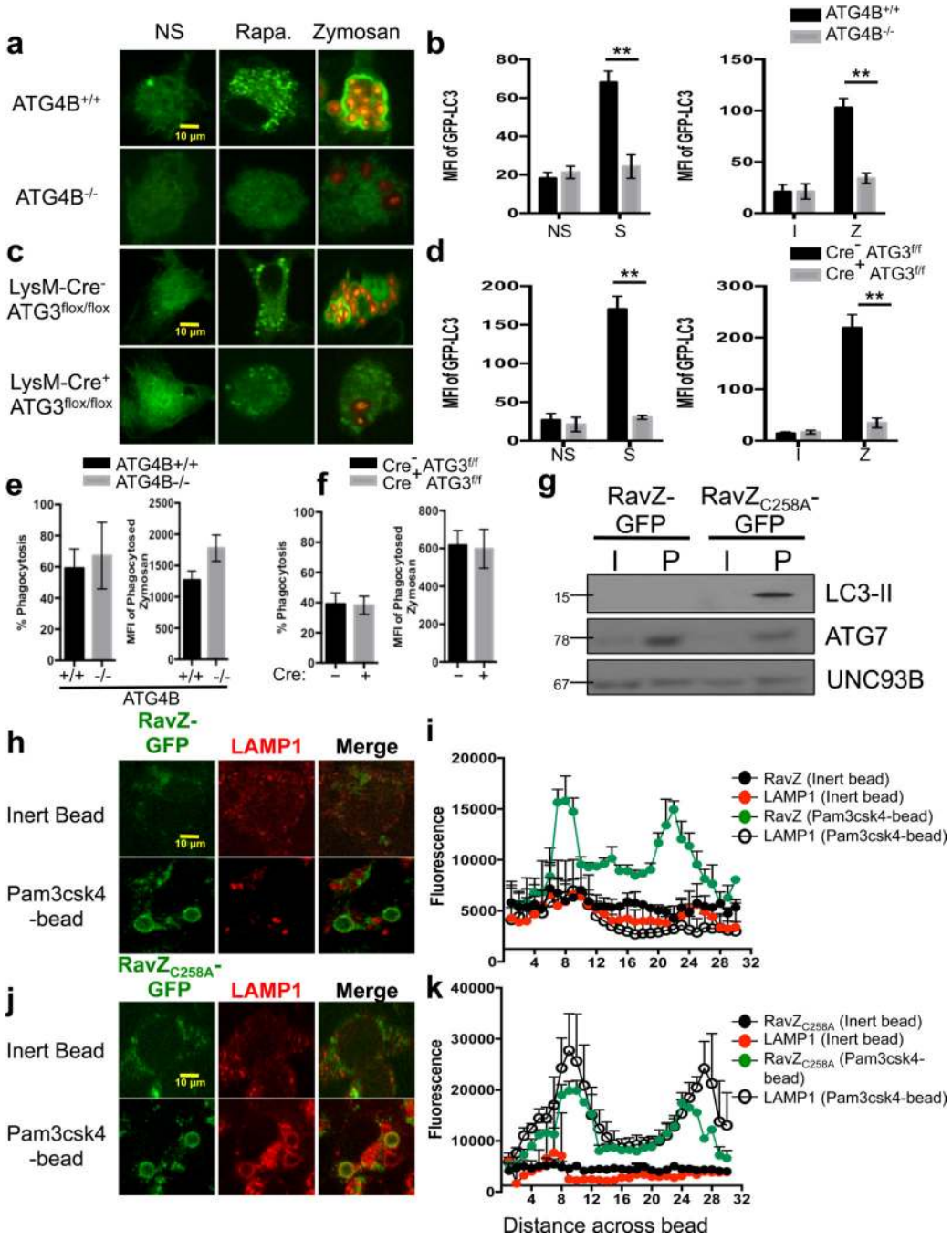

Figure 6. LAP-induced phagosome maturation requires LC3-II

(**a–b**) Bone marrow-derived macrophages from ATG4B$^{+/+}$ and ATG4B$^{-/-}$ mice were transfected with GFP-LC3. After 48 hours of transfection, cells were left untreated (NS) or were cultured with 200 nM rapamycin (Rapa., **a**), starvation conditions (S, **b**), Inert beads (I, **b**), or Alexa Fluor 594-zymosan (Zymosan or Z, **a–b**). (**c–d**) Bone marrow-derived macrophages from LysM-Cre– ATG3$^{flox/flox}$ and LysM-Cre+ ATG3$^{flox/flox}$ mice were transfected with GFP-LC3. After 48 hours of transfection, cells were left untreated (NS) or were cultured with 200 nM rapamycin (Rapa., **c**), starvation conditions (S, **d**), Inert beads (I,

d), or Alexa Fluor 594-zymosan (Zymosan or Z, **c–d**). GFP-LC3 puncta was assessed at 18 h, and translocation of GFP-LC3 to the LAPosome was assessed at 1 h by confocal microscopy (**a, c**) and flow cytometry (**b, d**). Data are presented as mean ± SD of three independent experiments (**p < 0.001). (**e–h**) RAW cells were transfected with RavZ-GFP (**e–f**) or $RavZ^{C258A}$-GFP (**g–h**). After 48 hours of transfection, cells were fed inert beads or Pam3csk4-beads for 1 hour. Immunofluorescent staining was performed for LAMP1 and analyzed by microscopy. Representative images (**e, g**) and signal intensity profiles (**f, h**) for RavZ, $RavZ^{C258A}$, and LAMP1 across phagocytosed beads are quantified and shown graphically (n ≥20 / genotype). Data are presented as mean ± SD of two independent experiments. (**i**) RAW cells were transfected with RavZ-GFP or $RavZ^{C258A}$-GFP. After 48 hours of transfection, cells were allowed to phagocytose inert beads or Pam3csk4-beads for 1 hour. Phagosomes were purified using sucrose gradient as described in experimental procedures. Phagosome proteins (left), as well as whole cell lysates from non-stimulated cells (right), were solubilized in SDS-PAGE and blotted with the indicated antibodies. The results presented are representative of three independent experiments.

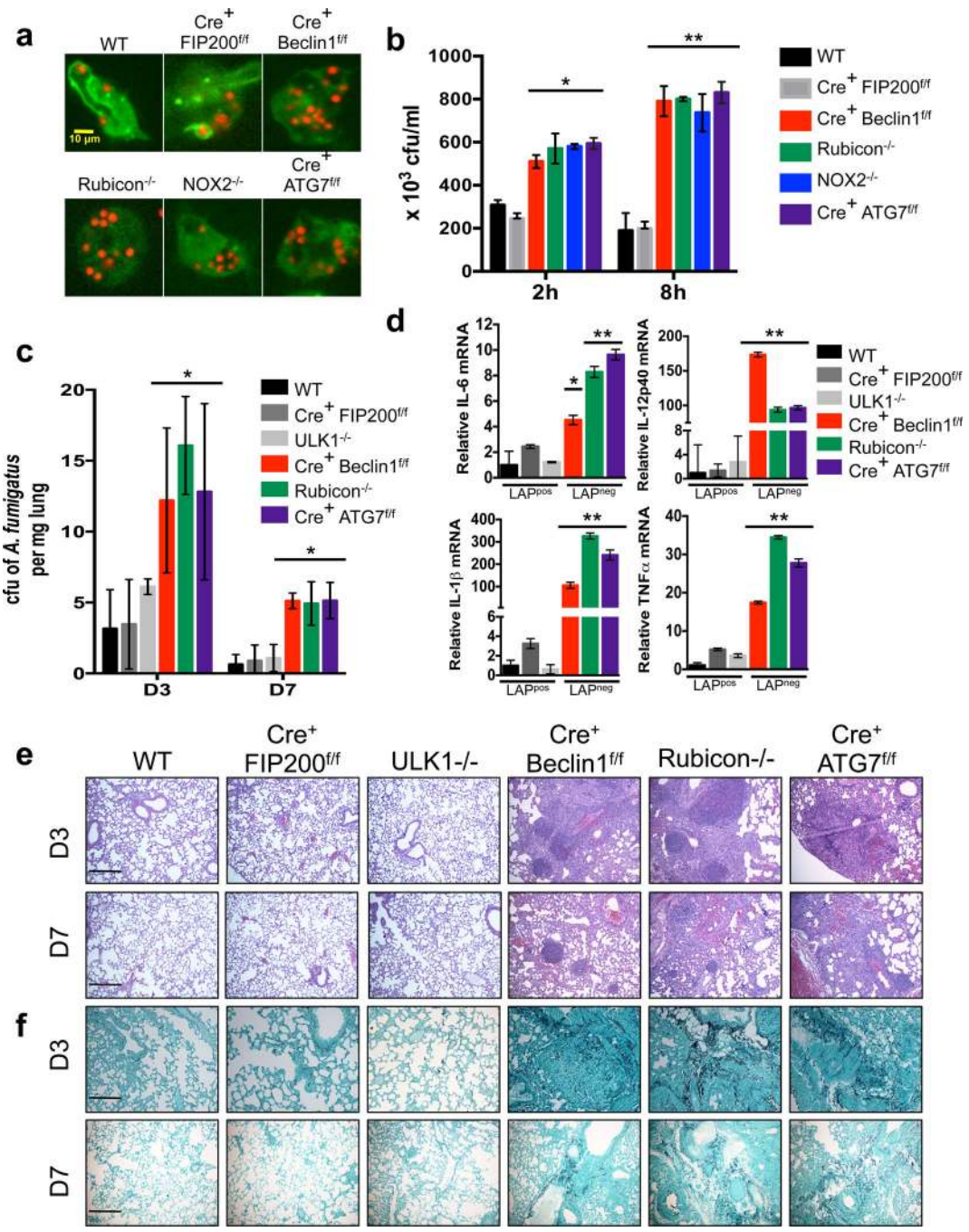

Figure 7. Clearance of *Aspergillus fumigatus* requires LAP

(**a**) Bone marrow-derived macrophages from GFP-LC3$^+$ genetic knockout strains were fed live *A. fumigatus*-dsRed at an MOI of 5, and translocation of GFP-LC3 to the LAPosome was assessed at 1 h by confocal microscopy. Representative images are shown (n ≥20 / genotype). (**b**) Bone marrow-derived macrophages from different genetic knockout strains were fed live *A. fumigatus* at an MOI of 1, and colony-forming units per ml (cfu/ml) of cell lysate was measured at 2 and 8 hours post-infection. Data are presented as mean ± SD of three independent experiments (*p< 0.05, **p < 0.01). (**c–f**) Mice of different genetic

knockout strains were infected intranasally with live *A. fumigatus* conidia. *A. fumigatus* cfu per mg of lung tissue was measured on days 3 and 7 post-infection (**c**). Relative mRNA levels of IL-6, IL-1β, IL-12p40, and TNFα in infected lung tissue homogenates at day 3 post-infection were quantified by real-time PCR. Data normalized to actin. Data are presented as mean ± SD of three independent experiments (*$p < 0.05$). Lung histopathology [H&E staining, (**e**) and Gomorri staining (**f**)] on days 3 and 7 post-infection. Representative images are shown of 10× magnification. Scale bars represent 100 μm.

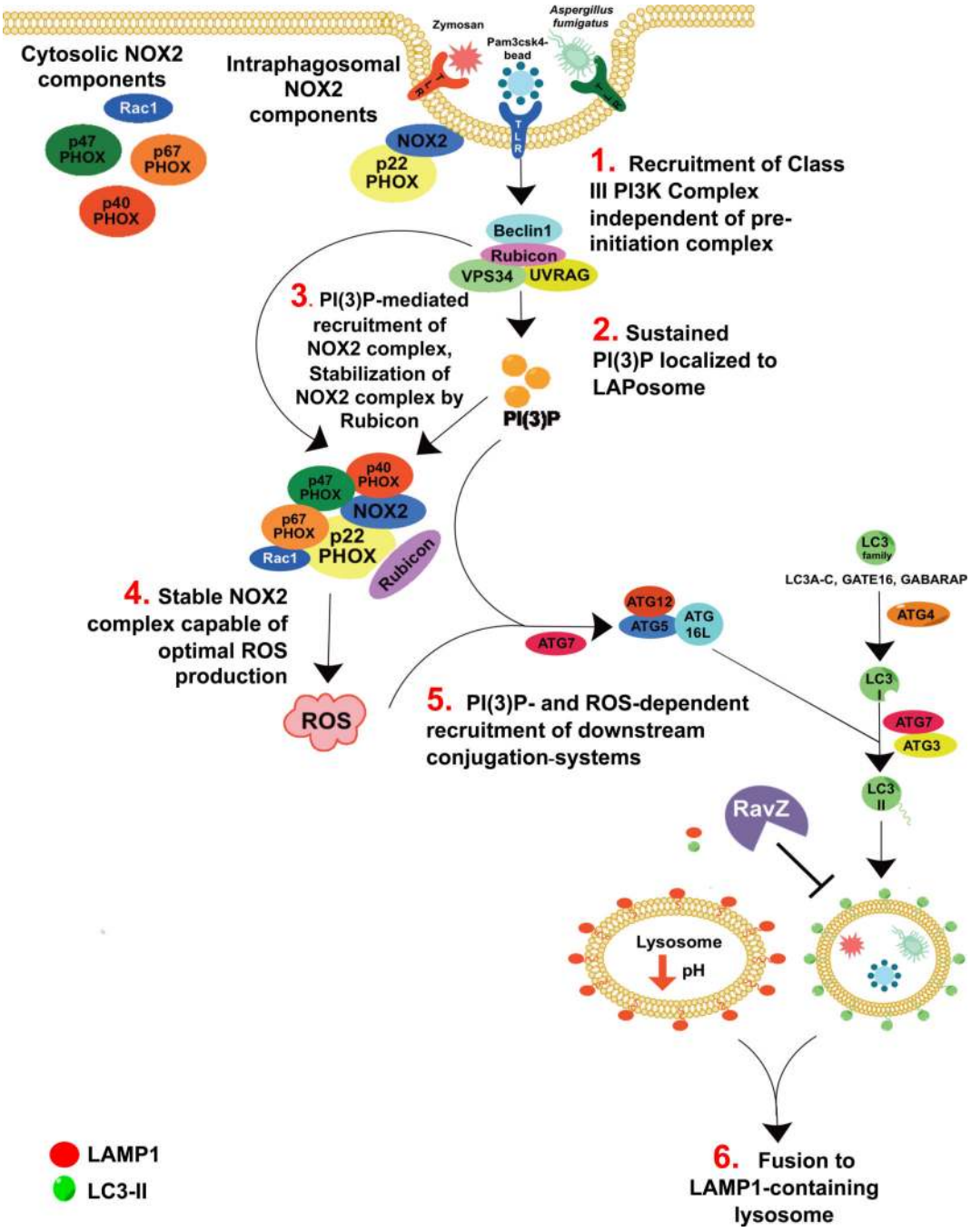

Figure 8. Proposed Model of LC3-Associated Phagocytosis

Recruitment of the Rubicon- and UVRAG-containing Class III PI3K complex allows for sustained VPS34 activity at the LAPosome, resulting in significant PI(3)P deposition on the LAPosome membrane. This PI(3)P allows for the recruitment of autophagic downstream conjugation systems to the LAPosome and stabilizes the NOX2 complex via its binding to p-p40PHOX. Rubicon itself also stabilizes the NOX2 complex, promoting optimal ROS production. Both PI(3)P and ROS are required for the recruitment of the downstream conjugation systems. LAP requires the activity of ATG5-ATG12-ATG16L complex, as well

as ATG3 and ATG4, all of which are critical to the lipidation of LC3. Importantly, the maturation of the LAPosome requires the presence of LC3-II, as macrophages that express the Legionella effector protease, RavZ, fail to mature into LAMP1^{+} LAPosomes.